

COMPACT INFRARED SOURCES ASSOCIATED WITH SOUTHERN H II REGIONS. II.

JAY A. FROGEL,*†‡ S. ERIC PERSSON,‡§ AND MARC AARONSON †‡

Received 1976 August 20; revised 1976 October 7

ABSTRACT

We have found extended sources of 10–20 μm emission to be associated with nine southern H II regions of high emission measure. Ten and 20 μm maps or scans and photometry from 1 to 20 μm are presented for most of these regions. NGC 3603, one of the most luminous H II regions in the Galaxy, possesses several noteworthy characteristics: the infrared emission from 2.2 to 20 μm shows good spatial coincidence with the H α emission; there is evidence that the young, luminous star cluster associated with the gas has a strong dynamical effect on the gas and dust; and several bright 2.2 μm point sources are associated with this complex.

Preliminary observations of the strength of a 20 μm silicate absorption feature yield an optical depth which is not more than one-third that of the 10 μm silicate feature. The energetics of H II regions are rediscussed in light of the observations of the 10 and 20 μm silicate features.

Subject headings: infrared: sources — nebulae: general

I. INTRODUCTION

This paper reports the discovery of 1–25 μm infrared sources associated with nine galactic H II regions. This brings to 22 the number of southern H II regions in which we have detected such infrared sources (Becklin *et al.* 1973*a*, 1974; Frogel and Persson 1974, hereafter Paper I). The nature of a twenty-third infrared emission source, OH 284.2–0.8, remains uncertain (Frogel and Persson 1975 and references therein; Caswell and Haynes 1975). Observations of the 10 μm silicate feature in most of these 23 objects have been discussed by Persson, Frogel, and Aaronson (1976, hereafter Paper II). Here we present detailed spatial data and additional spectral data for the nine new sources. These data include 10 μm maps for six of the sources and a comparison of the distributions of the 10 μm and 20 μm emission for several of them. Unfortunately, a severe lack of adequate radio data, especially high-resolution continuum maps, precludes a detailed comparison of the distributions of gas and dust.

Special emphasis is placed on NGC 3603, a giant H II region which has intense radio and optical emission and which contains an extremely compact cluster of highly luminous stars similar to 30 Doradus (Walborn 1973).

In addition to the broad-band photometry and maps, we also present preliminary observations of the 20 μm silicate feature in eight of the 23 sources. By combining

far-infrared observations with our near-infrared continuum and silicate absorption feature observations, we are able to rediscuss the energetics of IR/H II regions.

II. OBSERVATIONAL RESULTS

The data presented in this paper were obtained in 1974, 1975, and 1976 with the 1 m telescope at Las Campanas Observatory, Chile, with a Ge:Ga bolometer, PbS, and InSb systems. The instrumental setup, data-collecting techniques, and initial reduction are similar to those described in Papers I and II. Briefly, the beam separations and chopping directions were typically 73" or 134" north-south and 44" east-west for the short and long wavelengths, respectively. Contour maps at 10 μm for six of the H II regions were constructed using scans made with aperture diameters of 14.5 or 23". Integrated 10 μm flux densities for these regions were found by planimetry of the maps. For two sources, only central scans were made; the 10 μm flux densities were estimated by assuming circular symmetry and integrating under the scans. In Paper I this method was shown to produce satisfactory results for similar sources. The results are given in Table 1. Absolute positions were determined by offsetting from the infrared sources to field stars.

Preliminary measurements of eight sources with three intermediate bandwidth filters in the 20 μm window were made in an attempt to place limits on a silicate spectral feature which occurs between 19 μm and 20 μm . The central wavelengths and half-power bandwidths of these filters are 18.1, 1.6 μm ; 19.8, 1.7 μm ; 22.9, 2.3 μm . The absolute flux calibration for these filters is based on the 20 μm broad-band calibration of Becklin *et al.* (1973*b*). At 20 μm , the magnitude of η Car was found to be -9.4 , and magnitudes at the wavelengths of the three filters were derived by

* Cerro Tololo Inter-American Observatory, which is operated by the Association of Universities for Research in Astronomy, Inc., under contract with the National Science Foundation.

† Guest Investigator at Las Campanas Observatory, Carnegie Institution of Washington.

‡ Center for Astrophysics, Harvard College Observatory and Smithsonian Astrophysical Observatory.

§ Hale Observatories, Carnegie Institution of Washington, and California Institute of Technology.

TABLE 1
 Observed Properties of H II Regions

Galactic Source	Other Names	Radio† Position (1950.0)	10 μ† Position (1950.0)	Size*			Dist. kpc	log F _ν ‡		A _V	Molecules§	Notes	
				Radio FWHP (')	10 μ FWHP (")	20 μ FWHP (")		Radio ν (GHz)	10 μ				
G274.0-1.1	RCW 42	09 ^h 22 ^m 49 ^s -51°46'7"	09 ^h 22 ^m 45 ^s 5" -51°46'27"	2.2x2.1	24±4	22±5	6.5	-24.59	5	-23.94	15	OH(A), (11)	2,4,15
G282.0-1.2		10 04 53 -56 57.5	10 04 55.9 -56 57 56	2.0	38±6	38±6	7.0	-24.59	5	-24.02	15	no OH(A), (10)	1,6
G291.6-0.5	NGC 3603 RCW 57B	11 12 53 -60 59.4	11 12 50.8 -60 59 37	5	37±3	27±3	8.4	-23.76	5	-22.59	4	OH(A), (11)	1,3,6,13
G333.1-0.4		16 17 16 -50 29.2	16 17 14.6 -50 28 50	4	19±6	--	3.7	-24.38	5	-23.85	9	OH(A), (11)	1,3,7
G337.9-0.5		16 37 27 -47 01.6	16 37 27.1 -47 01 00	1.4	14±5	14±6	3.4	-24.76	5	-23.30	12	H ₂ O, (9) OH(E,A), (10,11,12)	1,6,14
G340.8-1.0	RCW 110B	16 50 39 -45 12.2	16 50 40.3 -45 12 32	0.8	35±12	35±12	2.5	-25.03	5	-24.22	20	no OH(E), (10) OH(A), (11)	1,6,15
G348.2-1.0	H2-6 RCW 121	17 14 56 -39 16 10	17 14 57.6 -39 16 16	--	32±5	32±6	5	-25.08	15	-23.63	6	no OH(E), (10) no OH(A), (11)	5,17
G348.7-1.0	RCW 122	17 16 39 -38 54.6	17 16 40.6 -38 54 18	1.9	24±4	24±6	5	-24.48	5	-23.25	11	no H ₂ O, (8) OH(E,A), (11)	1,5
G10.2-0.3	W31	18 06 23 -20 20.2	18 06 31.1 -20 20 10	2.1	--	--	9	-24.32	5	>-24.27	--		1,5,16

*The radio size is at the frequency in column (10). The infrared sizes are from the maps and central scans.

†Absolute 10 μ position error is 5-10"; radio position errors are typically ±1'.

‡These are spatially integrated values.

§A refers to absorption, E to emission. Emission is noted only if near radio and 10 μ position. Numbers refer to Notes below.

NOTES

1. Position from 5 GHz measurements of Goss and Shaver 1970. Radio size and flux density from Shaver and Goss 1970. Position uncertainty ±1'.
2. Position, size, and flux density from Caswell 1972.
3. 8.9 GHz size and flux density from McGee *et al.* 1975. These sizes are significantly smaller than those at 5 GHz.
4. Distance from Caswell *et al.* 1976.
5. Distance from Radhakrishnan *et al.* 1972.
6. Distance from Shaver and Goss 1970.
7. Distance from McGee *et al.* 1975.
8. Johnston *et al.* 1972.
9. Caswell *et al.* 1974.
10. Robinson *et al.* 1974.
11. Caswell and Robinson 1974.
12. Caswell and Haynes 1975.
13. Size refers to IRS-1. For IRS-2, we find 70" ± 12 and 50" ± 8 at 10 μm and 20 μm, respectively.
14. Size refers to IRS-1. For IRS-2, we find 40" ± 7 at both 10 and 20 μm.
15. Integrated 10 μm flux density is from central scan only.
16. For W31, F_ν (10 μm) is from a measurement with only one aperture.
17. 15 GHz flux and optical (not radio) position from Rubin 1970.

assuming that the energy spectrum of η Car can be represented by a 250 K blackbody.¹ The resulting magnitudes are -9.2, -9.4, and -9.7 at 18.1 μm, 19.8 μm, and 22.9 μm, respectively. Table 5 contains the measurements of the eight sources. Owing to uncertainties in the air-mass correction and the absolute calibration, 25% errors are attached to measurements at these wavelengths.

Table 1 identifies the new sources, compares the infrared and radio continuum positions and sizes, and lists other observed source properties. In all cases, the infrared and radio positions are in agreement. This

¹ This is not strictly true, since η Car has a weak emission feature at 10 μm and, thus, probably has one at 20 μm also. The conclusions drawn from the observations should not be significantly affected by this, however.

agreement is used to justify the intimate association of the infrared and radio emission sources. The values of A_v are those used in Paper II and are obtained by comparing the mean H-K color with that expected from ionized gas alone. Uncertainties in these values are probably ±5 mag (Paper II). Table 2 contains a representative sample of our broad-band photometric measurements corrected for flux in the reference beam. Note that the values of H-K in this table may differ from the mean values used to derive A_v. Energy distributions of some of the regions are displayed in Figure 1.

III. NGC 3603 (G291.6-0.5)

The radio observations of NGC 3603 (RCW 57 B) imply that it is one of the most massive ($M_{\text{H II}}/M_{\odot} \approx 1.4 \times 10^4$) and luminous H II regions in the Galaxy

TABLE 2
 Photometry of H II Regions*

Source	Aperture Near IR (")	[2.2 μ]	log F_{ν} (2.2 μ) ($\text{Wm}^{-2} \text{Hz}^{-1}$)	Colors			Aperture 10 & 20 μ (")	log F_{ν} (10 μ) ($\text{Wm}^{-2} \text{Hz}^{-1}$)	log F_{ν} (20 μ)
				J-H	H-K	K-L			
G274.0-1.1 (RCW 42)	29	7.67	-26.28	--	2.0 \pm 0.5	1.96	22	-24.42	-23.67
	58	6.92	-25.98	--	1.51	--			
G282.0-1.2	14	8.65	-26.67	1.55	1.00	1.36	14	-24.86	-24.24
G291.6-0.5/IRS 1 (NGC 3603)	22	8.36	-26.56	0.49	0.79	1.36	22	-23.91	-23.19
G333.1-0.4/IRS 1	29	6.83	-26.57	--	2.12	1.57	22	-24.66	-24.09
G333.1-0.4/IRS 3	29	4.54	-25.18	0.77	0.40	0.38	--	--	--
G337.9-0.5/IRS 1 G337.9-0.5/IRS 2	58	6.76	-25.91	1.63	1.34	--	22	-24.44	-23.62
							22	-24.66	-24.10
G340.8-1.0 (RCW 110B)	29	7.31	-26.13	--	1.79	1.62	29	-24.70	-24.04
G348.2-1.0/IRS 1 (H2-6)	14	9.72	-27.10	--	1.18	2.15	22	-24.64	-23.99
G348.2-1.0/IRS 3	14	7.78	-26.32	0.47	0.28	0.60	--	--	--
G348.7-1.0/IRS 1 (RCW 122)	14	9.50	-27.01	--	1.69	2.28	22	-24.09	-23.51
G10.2-0.3 (W31)	--	--	--	--	--	--	29	-24.27	-23.67

*Aperture was centered on region of maximum apparent surface brightness which may not correspond to positions indicated by maps because of complex source structure.

(Goss and Radhakrishnan 1969; Goss and Shaver 1970; Shaver and Goss 1970). Even though it is at a distance of somewhat more than 8 kpc (Goss and Radhakrishnan 1969; Moffat 1974), it is optically prominent. Asymmetrically placed with respect to the most intense parts of the nebula is an extremely compact cluster of highly luminous blue stars (Sher 1965; Moffat 1974). An $H\alpha$ photograph of the region obtained by N. Walborn on the Cerro Tololo Inter-American Observatory 4 m telescope is shown in Figure 2 (Plate 14). Several other photographs of the region may be found in Sher (1965) and Walborn (1973). Moffat's work yields a photometric distance in agreement with the kinematic distance (Table 1); gives a mean visual extinction of 4 mag for the cluster, abnormally low for the distance and galactic latitude; and shows that the most luminous stars are at least as bright as $M_v \approx -6$.

An OH maser source has been found about 6' north of the radio continuum peak (Robinson, Caswell, and Goss 1974), and OH absorption has been studied by Caswell and Robinson (1974). Recently, McGee, Newton, and Batchelor (1975) noted two 8.9 GHz components which appear to correspond with the two brightest optical and infrared components—one to the southwest, the other to the south and slightly east of the cluster. We associate these with the 10 μm sources IRS-1 and IRS-2 (see below).

Our infrared data for NGC 3603 consist of 10 μm and 20 μm maps, 2.2 μm scans, photometry of the brightest 10 μm source, photometry of the cluster itself, and photometry of several stellar sources in the vicinity of the extended radio and infrared sources.

a) The Extended 10 μm and 20 μm Emission

An area of 4' \times 4' centered on the cluster was scanned at 10 μm with a 14.5 diameter aperture. The only region with significant 10 μm emission is shown on the maps in Figures 2 and 3. Emission from the region scanned to the north and east of the cluster has a maximum surface brightness less than half that implied by the lowest contour level shown. There may be faint extended emission at the same level as that of the lowest contour to the northwest of the cluster.

One may immediately draw four conclusions from inspection of the 10 μm and 20 μm maps and the $H\alpha$ photograph in Figures 2 and 3. (1) The spatial distribution of the infrared emission is qualitatively similar to that of the $H\alpha$ emission; in particular, note the trough running away from the cluster to the southwest on both maps and the photograph. (2) The cluster itself is relatively free of diffuse $H\alpha$ emission and 10 μm and 20 μm emission. (3) The 20 μm emission is more sharply peaked than is the 10 μm emission. This trend, especially noticeable in IRS-1, implies that the cores of the sources have lower color temperatures than the extended background emission. (4) The surface-brightness gradient is steepest on the side of IRS-1 facing the cluster.

The region of strong 10 μm emission was also scanned in declination with a 22" diameter aperture at 2.2 μm . These scans show qualitatively the same features as appear on the 10 μm and 20 μm maps and on the $H\alpha$ photograph. In particular, the relatively steep emission gradient on the cluster side of the sources is apparent. Within the IR/H II region itself, only one distinct

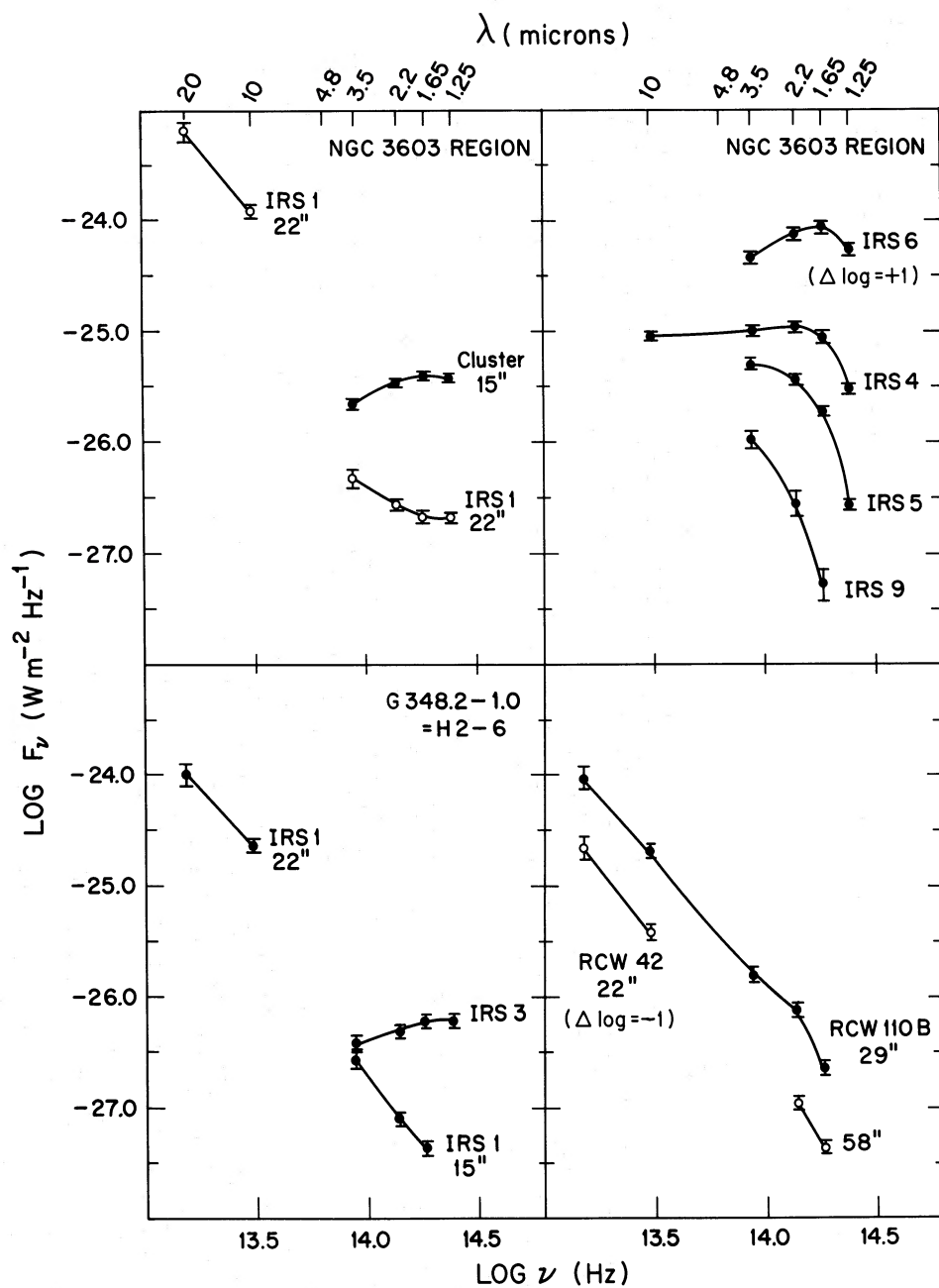


FIG. 1.—Representative spectral energy distributions for H II regions and stars associated with NGC 3603. The measurements have been corrected for the extended nature of the sources, and the measuring aperture diameters noted. Energy distributions for the other sources in this paper are given in Tables 2 and 3.

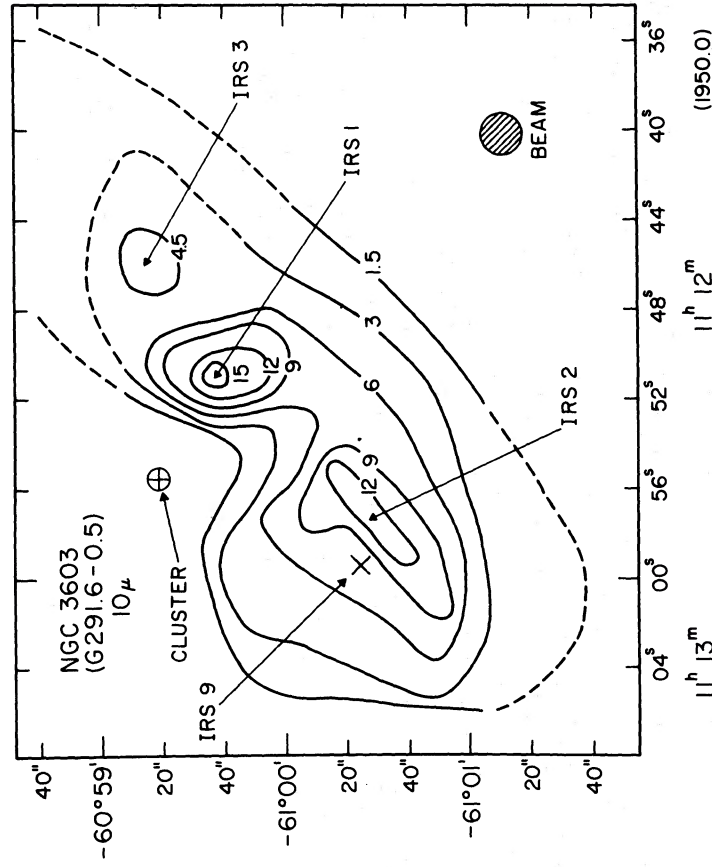
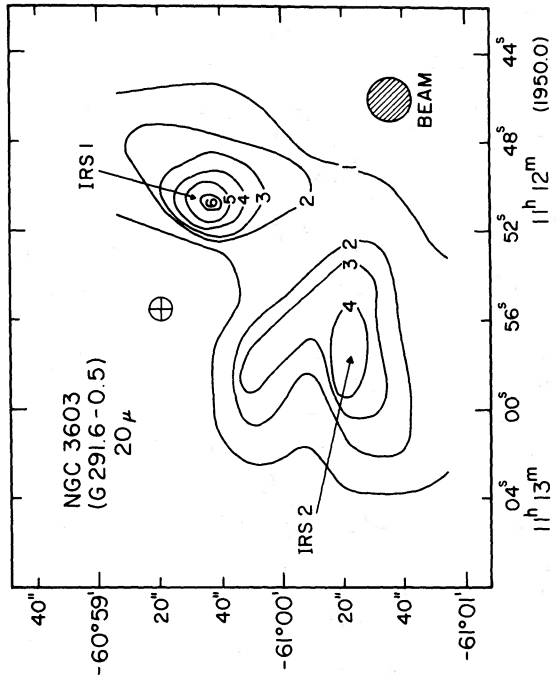


Fig. 3.—Ten and 20 μm maps of the NGC 3603 (G291.6-0.5) region assembled from scans made with a $14''.5$ diameter aperture. The peak contours, 15 and 6, correspond to $6.7 \times 10^{-25} \text{ W m}^{-2} \text{ Hz}^{-1}$ ($10 \mu\text{m}$) and $3.8 \times 10^{-24} \text{ W m}^{-2} \text{ Hz}^{-1}$ ($20 \mu\text{m}$) as measured with a $14''.5$ diameter aperture. The $2.2 \mu\text{m}$ source IRS-9 is discussed in the text. The dashed lines indicate uncertainty in location of the contours because of low signal-to-noise ratio.

TABLE 3
POSITIONS AND PHOTOMETRY OF OBJECTS IN THE VICINITY OF THE CLUSTER NGC 3603

Source	α (1950.0)	δ (1950.0)	$[2.2\mu]^\dagger$	$\log F_\nu$ (2.2μ) ($\text{Wm}^{-2} \text{Hz}^{-1}$)	COLORS [†]			NOTES
					J - H	H - K	K - L	
NGC 3603	11 12 ^m 55.7 ^s	-60° 59' 21"	5.50	-25.41	0.43	0.29	0.42	1
			5.73	-25.50	0.45	0.27	0.38	2
G291.6-0.5	11 12 53	-60 59.4	3
OH	11 12 54.1	-60 53 08	4
IRS 1	11 12 50.8	-60 59 37	8.36	-26.56	0.49	0.79	1.36	1, 5
IRS 2	11 12 57.1	-61 00 30	
IRS 4	11 12 52.3	-60 58 08	4.39	-24.97	1.63	0.71	0.76	6
IRS 5	11 12 40.4	-60 57 38	5.54	-25.43	2.57	1.24	1.17	
IRS 6	11 13 14.3	-60 57 26	4.76	-25.11	1.00	0.33	0.30	
IRS 7	11 12 48.6	-61 03 07	9.09	-26.85	1.23	0.71	...	
IRS 8	11 12 57.9	-60 59 43	7.74	-26.30	0.50	0.30	0.36	
IRS 9	11 12 59.4	-61 00 25	8.40	-26.57	...	2.1(±0.3)	2.3(±0.2)	
IRS 12	11 12 47.1	-61 00 58	8.58	-26.64	0.78	0.12	...	7
IRS 13	11 12 42.8	-61 02 14	8.02	-26.42	1.17	0.34	0.38	
IRS 14	11 12 51.2	-60 59 22	8.82	-26.74	0.37	0.70	...	
IRS 15	11 13 13.7	-60 55 45	6.74	-26.55	1.11	0.35	0.27	

†Errors for magnitudes and colors in this table are typically ± 0.05 mag.

NOTES

1. Measurements made with 22" diameter aperture.
2. Measurements made with 14" diameter aperture.
3. Radio continuum position from Goss and Shaver 1970.
4. OH position from Robinson *et al.* 1974.
5. 10 μm and 2 μm positions agree to within ± 5 arcsec. Absolute positions for the infrared sources may be in error by as much as ± 10 arcsec; relative positions, by ± 5 arcsec.
6. A 10 μm measurement of IRS-4 gives $[10 \mu\text{m}] = +1.66 \pm 0.15$, $\log F_\nu$ (10 μm) = $-25.04 \text{ W m}^{-2} \text{ Hz}^{-1}$.
7. IRS-10 and IRS-11, two faint sources found on drift scans, were not measured photometrically.

2.2 μm point source was found (limiting K -magnitude ≈ 9). This source, designated IRS-9, is discussed below.

The near-infrared colors of IRS-1 are given in Table 3, and the energy distribution is shown in Figure 1. The observed $J-H$ and $H-K$ colors are quite close to those expected for a nebula at 10^4 K, but if corrected for the amount of reddening associated with the cluster, viz., $E_{B-V} = 1.32$ (Moffat 1974), they appear too blue and could indicate the presence of either direct or scattered starlight. If there are early-type stars embedded in IRS-1 which produce the somewhat blue $J-H$ and $H-K$ colors, it is easy to show that they make only a small ($\sim 5\%$) contribution to the energy output of the region.

b) Integrated Photometry of the Cluster

Integrated photometric measurements of the cluster were made with 14.5 and 22" diameter apertures

(Table 3). If the observed infrared colors are dereddened by an amount consistent with the $B-V$ excess (Moffat 1974) via van de Hulst's curve number 15 (Johnson 1968), the resulting colors, viz., $J-K = 0.09$ and $K-L = +0.25$, are not consistent with what would be expected for early O stars, and cannot, in fact, be synthesized from a combination of colors of blue and red stars. Either there is anomalous reddening near the cluster core, or there is excess emission at 3.5 μm . Perhaps the known Wolf-Rayet star (HD 97950), which lies within the cluster, is responsible for the anomalous colors.

c) Unresolved 2.2 μm Sources

A region larger than that scanned at 10 μm was scanned at 2.2 μm with a 1' diameter aperture. These scans revealed several bright 2.2 μm sources, whose positions, magnitudes, and near-infrared colors are given in Table 3. Multiaperture photometry and scans

TABLE 4
INTRINSIC COLORS AND PROPERTIES OF
FOUR SOURCES NEAR NGC 3603

Source	Dereddened Color			CO Index	A_V	M_K	Estimated Spectral Type
	J - H	H - K	K - L				
IRS 4	0.89	0.32	0.43	0.30	7.7	-10.9	M Ib
IRS 5	0.89	0.32	0.47	0.33	16.3	-10.5	M Ib
IRS 6	0.59	0.11	0.13	0.28	~4	-10.2	K Ia-ab
IRS 15	0.70	0.13	0.10	0.16	~4	-8.2	K Iab-b

of most of them showed that they are unresolved at the shorter wavelengths. There is, at present, no direct evidence for the association of any of these objects with NGC 3603; in fact, with the exception of the brightest sources, which are discussed below, the number of fainter sources found may be consistent with what would be expected for a random region of the same size scanned in the galactic plane.

Spectra and additional photometric data for the four brightest sources are given in Figure 1 and Table 4. From their locations in a $J-H$, $H-K$ two-color diagram, the four brightest sources appear to be heavily reddened late-type stars. Let us first assume that they are associated with NGC 3603 and hence are at a distance of 8.6 kpc. The tabulations by Johnson (1966) and Lee (1970) show that the intrinsic $J-H$ colors of late K and M giants and supergiants are similar. Corrections to the observed colors and K -magnitudes of IRS-4 and IRS-5 for the implied amount of reddening and absorption lead to the values in Table 4. From the intrinsic $V-K$ colors given by Johnson (1966) and Lee (1970) and the absolute K -magnitudes of Table 4, the absolute visual magnitude-spectral type of calibration of Blaauw (1963) can be used, and we find consistency with the assumption that IRS-4 and IRS-5 are M supergiants at the distance of NGC 3603. Furthermore, the $K-L$ colors (and the $10\ \mu\text{m}$ magnitude of IRS-4—see Table 3) exhibit excesses which are typical for these late-type, high-luminosity stars. Since the colors of IRS-6 and IRS-15 are considerably bluer than those of IRS-4 and IRS-5, it was necessary to assume a minimum value for A_V of 4 mag—the value found from visual observations of the cluster. The dereddened colors, magnitudes, and spectral types for IRS-6 and IRS-15 are then found by the same procedure. Finally, CO and H_2O indices, which are sensitive functions of luminosity and temperature for late-type stars (Baldwin, Frogel, and Persson 1973) were also measured for these sources. The corrected values of these indices are seriously affected by small uncertainties in the reddening correction, and are not accurate to better than ± 0.07 mag. The resulting values are consistent, however, with the

interpretation that these four sources are K and M supergiants at a distance of 8 kpc.²

NGC 3603/IRS-9 is the reddest of the point sources found. The data presented in Figure 1 and Table 3 were corrected for the nebular background by using the scans and photometry in its immediate vicinity. The colors are not consistent with those of a normal, heavily reddened, early- or late-type star, but are similar to those of IRC +10011 and IRC +50137 (Hyland *et al.* 1972), two late-type, long-period variables with thick circumstellar shells. Alternatively, the $1.65\text{--}3.5\ \mu\text{m}$ energy distribution (corrected for the extinction of $A_V = 4$ mag) can be fitted by a 980 K blackbody having a luminosity of $10^3 L_\odot$. The nature of IRS-9 is thus quite uncertain, as is its association with NGC 3603.

d) Discussion

The current model for an IR/H II region (reviewed by Wynn-Williams and Becklin 1974) has most of the radiation shortward of $20\ \mu\text{m}$ arising from dust mixed with the ionized gas. This complex is embedded in a more extensive neutral region, which is the seat of far-infrared and molecular emission and which usually causes a considerable amount of local extinction ($A_V = 15$ to 50 is a typical range). Thus there is often little correspondence between the near-infrared appearance and the optical appearance of H II regions. If this model is appropriate for NGC 3603, then the correspondence between the infrared and the optical appearance of the nebula implies that there is no thick neutral circumnebular cloud along the line of sight to the brightest parts of the H II region. Some other examples of this situation are provided by W22 (Paper I) and H2-6 (this paper).

It is reasonable to assume that the many early O-type stars in the cluster provide the main energy source for this H II region. In fact, if this were not the case, the radio luminosity would require as many as 15 to 20 additional O4 stars to be hidden away. The $2.2\ \mu\text{m}$ scans of the region do not reveal the presence of such a collection of stars (see § IIIa). Thus it is notable that the cluster is distinctly separated from the region of brightest infrared and $\text{H}\alpha$ surface brightness. However, on a smaller scale, W3 presents a similar picture (Wynn-Williams, Becklin, and Neugebauer 1972): W3/IRS-2, which appears to be an early-type star responsible for the excitation of at least radio component W3 A, is separated from the region of maximum radio surface brightness and its infrared counterpart W3/IRS-1 (cf. Churchwell 1974).

The morphology of the region thus points to the possibility that radiation pressure and/or stellar winds from the luminous cluster stars have driven most of the gas and dust away from the immediate vicinity of

² There are calibration differences between the present narrow-band indices and those of Baldwin, Frogel, and Persson (1973). The latter values of the CO index must be increased by 0.05 mag to correspond with those given here. The complete details of the H_2O transformation are not yet known, so the values for this index are not given.

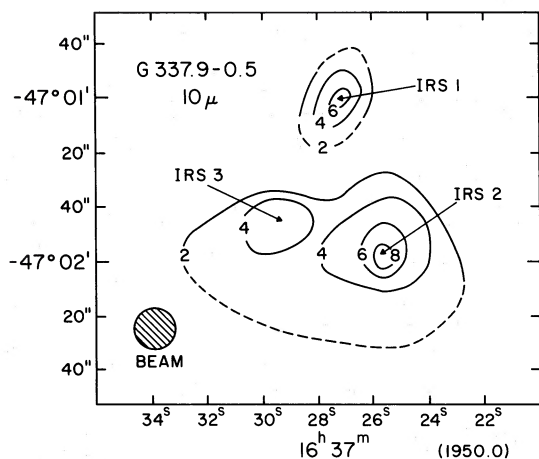


FIG. 4.—A $10\ \mu\text{m}$ map of G337.9-0.5. The peak contour 8 corresponds to $3.4 \times 10^{-25}\ \text{W m}^{-2}\ \text{Hz}^{-1}$ as measured with a $14\frac{1}{2}$ diameter aperture. The dashed lines indicate uncertainty in location of the contour because of low signal-to-noise ratio.

the cluster. Such a dynamical model for young stellar associations has been discussed recently by Elmegreen and Lada (1976). This process can also be invoked to account for the steep gradient in flux at $\text{H}\alpha$, $2.2\ \mu\text{m}$, and $10\ \mu\text{m}$ on the cluster side of IRS-1. The $10\ \mu\text{m}$ and $20\ \mu\text{m}$ maps show that IRS-1 has a lower color temperature than its surroundings. This situation, in which a condensation near a source of excitation is cooler than its surroundings even though the latter may be farther away from the source, is reminiscent of the Bar in Orion (Becklin *et al.* 1976). These observations could be accounted for if the heating of the inner parts of the condensation were lower than that of the outer parts because of extinction effects. A change in the relative numbers of large and small particles between the inside and outside would act in the same manner.

IV. PROPERTIES OF EIGHT OTHER SOURCES

a) G337.9-0.5 and RCW 122 (G348.7-1.0)

These two sources are considered together because they both show spatial variations in their $10\text{--}20\ \mu\text{m}$ color temperatures. The $10\ \mu\text{m}$ map of G337.9-0.5 is presented in Figure 4. What is most remarkable about this source is the change in the ratio of peak 10 to $20\ \mu\text{m}$ flux density as one proceeds in a north-south direction (Fig. 5). Photometry at several points confirmed these changes. That these observations cannot be accounted for by a variation in the $9.8\ \mu\text{m}$ silicate optical depth was shown in Paper II, where $\tau(9.8\ \mu\text{m})$ was found to be similar for IRS-1 and IRS-2.

The $10\ \mu\text{m}$ emission from RCW 122 arises from a region which coincides with some heavily obscured nebulosity. Figures 6 and 7 display the $10\ \mu\text{m}$ map and $10\ \mu\text{m}$ and $20\ \mu\text{m}$ scans. Although the color temperature change is considerably less striking than that in G337.9-0.5, it too was confirmed by photometry on the individual peaks.

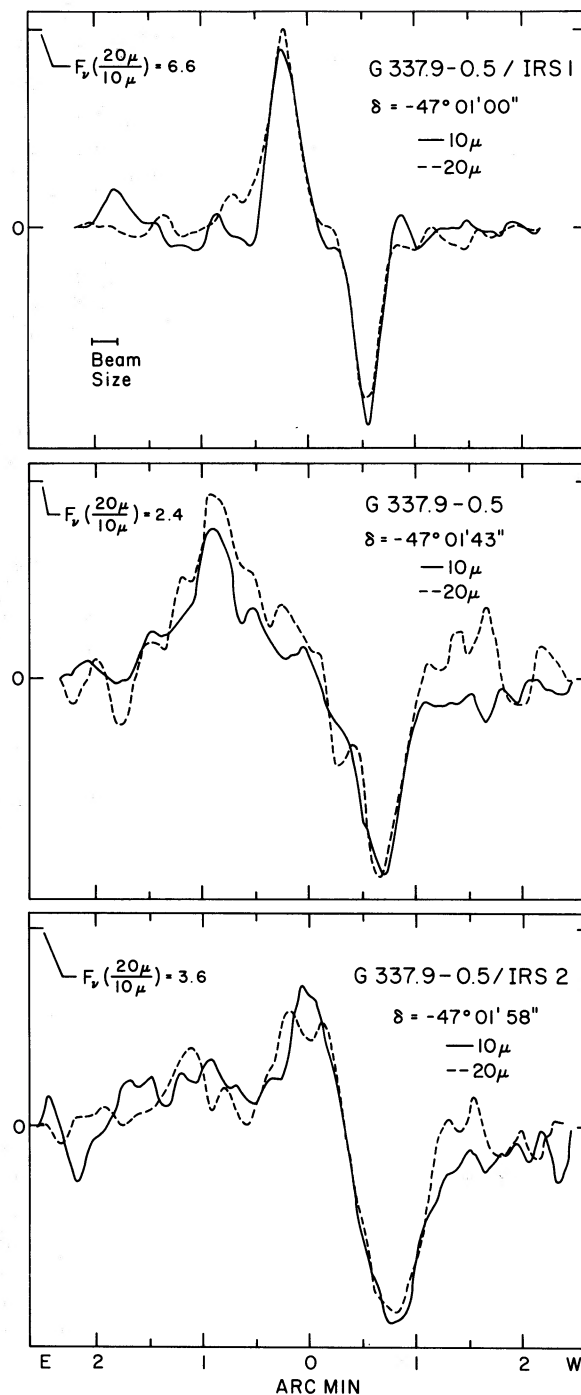


FIG. 5.—Representative $10\ \mu\text{m}$ and $20\ \mu\text{m}$ raw scans through G337.9-0.5. The scans have been drawn normalized to each other, and the ratios of the peak $20\ \mu\text{m}$ and $10\ \mu\text{m}$ flux densities are indicated. These show the change in color temperature across the source.

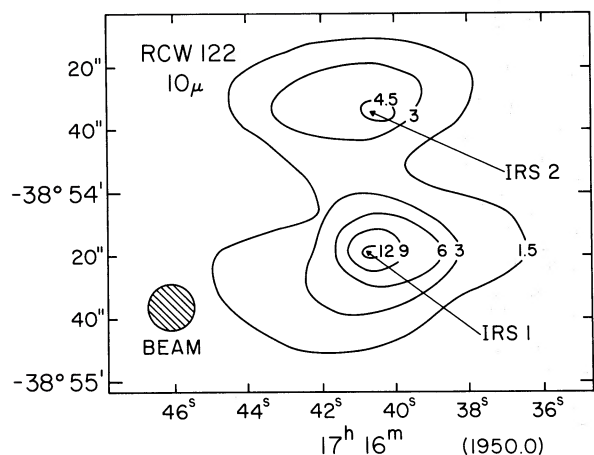


FIG. 6.—A $10\ \mu\text{m}$ map of RCW 122 (G348.7-1.0). The peak contour 12 corresponds to $5.3 \times 10^{-26}\ \text{W m}^{-2}\ \text{Hz}^{-1}$ as measured with a $14.5''$ diameter aperture.

b) H2-6 (G348.2-1.0), G333.0-1.2,
and G333.1-0.4

These are three similar, rather unremarkable H II regions. H2-6 was first detected as a moderate radio

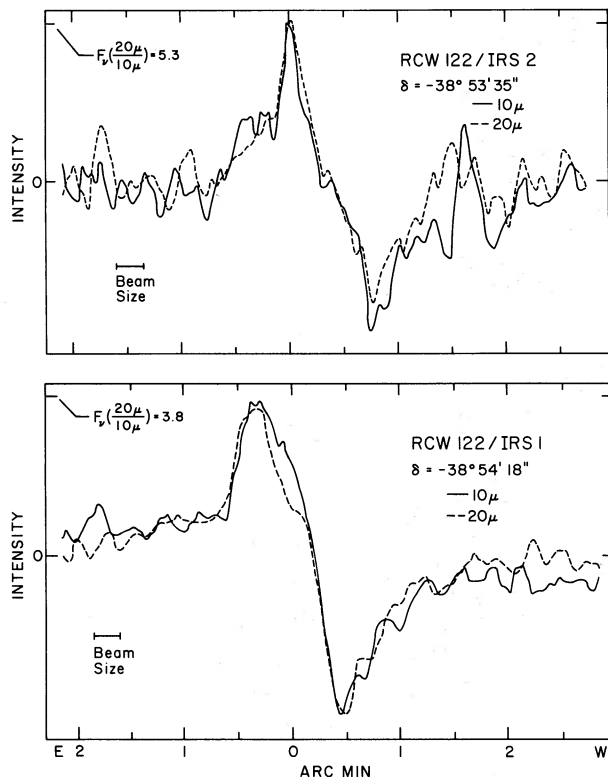


FIG. 7.—Representative $10\ \mu\text{m}$ and $20\ \mu\text{m}$ raw scans through RCW 122 (G348.7-1.0). The scans have been drawn normalized to each other, and the ratios of the peak $20\ \mu\text{m}$ and $10\ \mu\text{m}$ flux densities are indicated. As for G337.9-0.5, the scans also show the change in color temperature across the source.

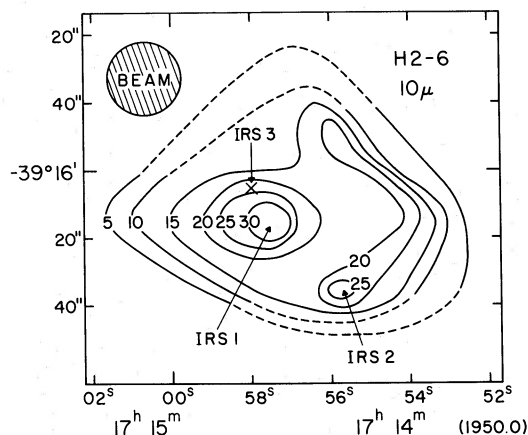


FIG. 8.—A $10\ \mu\text{m}$ map of H2-6 (G348.2-1.0). The peak contour 30 corresponds to $2.9 \times 10^{-26}\ \text{W m}^{-2}\ \text{Hz}^{-1}$ as measured with a $23''$ diameter aperture. The correspondence of the $2.2\ \mu\text{m}$ source IRS-3 and the nebulosity to optical counterparts is discussed in the text. The dashed lines indicate uncertainty in location of the contour because of low signal-to-noise ratio.

source by Beard, Thomas, and Day (1969), and was identified as a compact H II region with an optical counterpart by Rubin (1970). Aside from a distance determination by Radhakrishnan *et al.* (1972), no other significant radio work has been done on this source. A $10\ \mu\text{m}$ map of H2-6 is presented in Figure 8. The structure of the region at $10\ \mu\text{m}$ is similar to that in the visible as shown by the photograph in the *Catalogue of Galactic Planetary Nebulae* (Perek and Kohoutek 1967, hereafter *CGPN*). Figure 9 displays central scans at $10\ \mu\text{m}$ and $20\ \mu\text{m}$ which, to within the noise, are the same. In addition to the $10\ \mu\text{m}$ map, a limited area around H2-6 was scanned at $2.2\ \mu\text{m}$, and one bright ($K = 7.78$) source (IRS-3) was found. Its location corresponds to that of a star visible on the eastern edge of the nebulosity. The ($J-H$) and

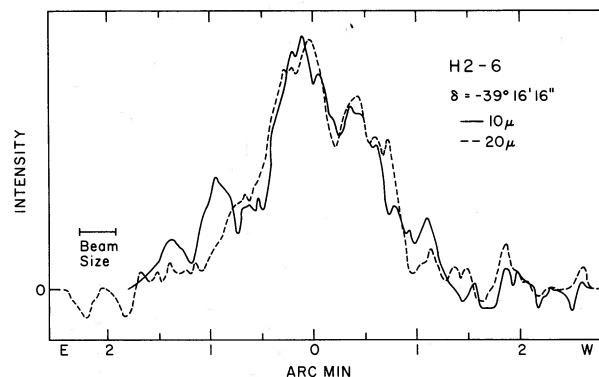


FIG. 9.—Ten and $20\ \mu\text{m}$ deconvolved scans through H2-6 (G348.2-1.0) showing the similarity in source structure at these wavelengths. A $23''$ diameter aperture was used. The $10\ \mu\text{m}$ scan was *not* that used in constructing the $10\ \mu\text{m}$ map of Fig. 9, since $20\ \mu\text{m}$ scans were not made on the night the $10\ \mu\text{m}$ map was made. The peak intensities of the scans have been normalized.

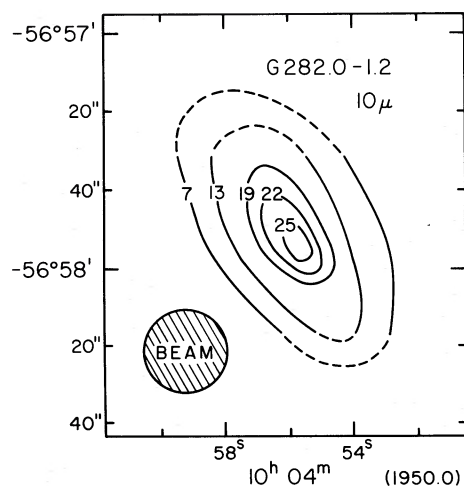


FIG. 10.—A $10\ \mu\text{m}$ map of G282.0-1.2. The peak contour 25 corresponds to $2.4 \times 10^{-25}\ \text{W m}^{-2}\ \text{Hz}^{-1}$ as measured with a $23''$ diameter aperture. The dashed lines indicate uncertainty in location of the contour because of low signal-to-noise ratio.

($H - K$) colors of H2-6/IRS-3 (Table 2) are consistent with its being an O star with $A_v = 6.1$ mag and $V = 13$. This magnitude, in turn, is consistent with its appearance in the *CGPN*. Also, the extinction agrees with that determined from the nebular emission (Table 1). The resulting M_v is -7.2 if the distance in Table 1 is assumed. Although this is high for normal O stars, we note that the radio-determined distance could be overestimated by nearly a factor of 2 (Radhakrishnan *et al.* 1972). This fact, together with the observation that the dilution factor may be ~ 4 for a star situated where IRS-3 is with respect to the nebula,

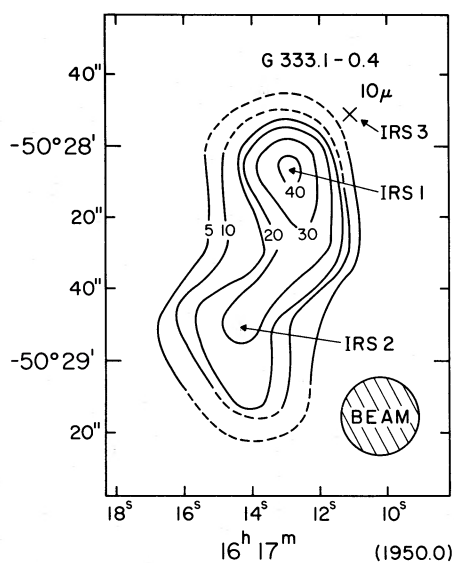


FIG. 11.—A $10\ \mu\text{m}$ map of G333.1-0.4. The peak contour 40 corresponds to $3.9 \times 10^{-25}\ \text{W m}^{-2}\ \text{Hz}^{-1}$ as measured with a $23''$ diameter aperture. The $2.2\ \mu\text{m}$ source IRS-3 is discussed in the text. The dashed lines indicate uncertainty in location of the contour because of low signal-to-noise ratio.

means that if the two are physically associated there need not be any inconsistency between the luminosity of the star and the energy requirements of the infrared-radio source (see Table 6). Multiaperture photometry of IRS-3 makes it likely that the red $K-L$ color arises from a nebular contribution to the $3.5\ \mu\text{m}$ flux density.

G282.0-1.2 and G333.1-0.4 were selected from the lists of Goss and Shaver (1970) and Shaver and Goss (1970). Maps at $10\ \mu\text{m}$ of these sources are in Figures 10 and 11, respectively. In addition to the $10\ \mu\text{m}$ map of G333.1-0.4, a few $2.2\ \mu\text{m}$ scans were made in the vicinity of the $10\ \mu\text{m}$ source. These revealed a very bright (Table 2) point source IRS-3 just to the northwest of IRS-1. A $0.94\ \mu\text{m}$ image-tube photograph of the region (Cohen and Frogel 1976) reveals a bright object at the position of IRS-3. No other object within a $10'$ radius of G333.1-0.4 is as bright or as red as this source. If, as for H2-6, we assume that IRS-3 is an early-type star, then the $J-H$, $H-K$, and $K-L$ colors are consistent with an A_v of between 8.8 and 10.6 mag. Again, this agrees with the value deduced from the nebular emission (Table 1). The resulting M_v , if the distance is as given in Table 1, is -9.6 , an unreasonable value for a normal O star. If, on the other hand, we assume that IRS-3 is an early K giant, the extinctions derived from the $J-H$ and $H-K$ colors are grossly inconsistent ($A_v = 1.6$ and 5.4 mag, respectively) unless this object possesses a circumstellar shell with an excess at $2.2\ \mu\text{m}$. Thus the nature of this object and its association with the H II region are unclear.

c) RCW 42 (G274.0-1.1), RCW 110 B (G340.8-1.0), and W31 (G10.2-0.3)

Time limitations and/or nights of excessive $10\ \mu\text{m}$ noise prevented us from making complete maps of these three sources. RCW 42 (G274.0-1.1) was found to be a strong radio source by Caswell (1972). Subsequently, it has been observed at 8.9 GHz by McGee, Newton, and Batchelor (1975). Central $10\ \mu\text{m}$ and $20\ \mu\text{m}$ scans (Fig. 12) are sensibly the same.

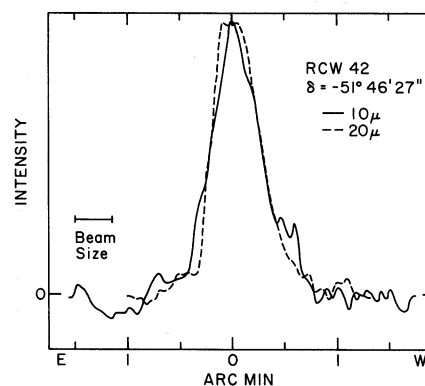


FIG. 12.—Ten and $20\ \mu\text{m}$ deconvolved scans through RCW 42 showing the similarity in source structure at these wavelengths. A $23''$ diameter aperture was used. The peak intensities of the scans have been normalized.

TABLE 5
INTERMEDIATE-BAND PHOTOMETRY
NEAR 20 μ

Source	LOG F_{λ} ($\text{Wcm}^{-2} \mu^{-1}$)			
	12.6 μ	18.1 μ	19.8 μ	22.9 μ
G268.0-1.1	-15.19	-14.87	-14.81	-14.77
OH284.2-0.8	-15.23	-15.04	-15.03	-14.93
G291.3-0.7	-15.29	-15.16	-15.17	-15.11
G291.6-0.5	-15.47	-15.18	-15.22	-15.20
G298.2-0.3	-15.18	-14.99	-14.98	-14.88
G333.6-0.2	-14.41	-14.40	-14.45	-14.45
G337.9-0.5	-15.87	-15.59	-15.49	-15.23
G351.6-1.3	-15.73	-15.77	-15.77	-15.61

RCW 110 B is associated with some faint nebulosity about 5' south of RCW 110. The only new data we have for this source are the photometry in Table 1 and a mediocre 10 μm central scan from which we have estimated the full width at half-power (FWHP). W31 is a source which we were unable to locate previously (Paper I). The new data consist primarily of those presented in Paper II plus the photometry in Table 2.

V. THE 20 μm SILICATE FEATURE

Table 5 gives the fluxes measured for eight sources with the three intermediate bandwidth filters in the 20 μm window (OH 284.2-0.8 has been included). We have estimated apparent extinctions by defining a baseline between the 12.6 μm and 22.9 μm points and measuring how far below this the 18.1 μm and 19.8 μm fluxes lie. The 20 μm silicate feature measured at higher spectral resolution in several other H II regions appears to be about 2.5 μm wide, centered between 18.5 μm and 20 μm (Houck 1976). Thus the observed depressions of the 18.1 μm or 19.8 μm fluxes should yield a relative measure of the depth of the 20 μm feature. From the data of Houck (1976), we note that these values will underestimate the real depth by about a factor of 2. Figure 13 shows a plot of $\tau(9.8 \mu\text{m})$ values from Paper II against the apparent depressions at 18.1 μm and 19.8 μm . Although there is considerable scatter, the trend goes in the expected sense. Tentatively, we conclude that the apparent absorption near 20 μm is probably $\leq \frac{1}{3}$ that at 10 μm . To relate the true absorptions at 10 μm and 20 μm , knowledge of the underlying emission spectrum is required, and this is lacking at present. However, since the underlying emission is expected to be stronger at 10 μm than at 20 μm , the true absorption ratio $\tau(20 \mu\text{m})/\tau(9.8 \mu\text{m})$ is probably somewhat less than one-third. This result, although crude, agrees with the findings of Houck (1976).

VI. THE ENERGETICS

Previous considerations of the 1-25 μm luminosities of H II regions have not taken into account the absorption at 10 μm and 20 μm due to silicates (e.g., Paper I:

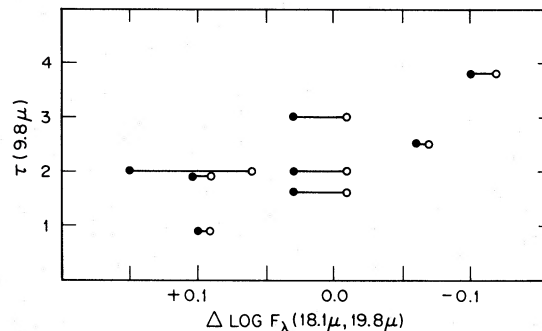


FIG. 13.—The relation between 9.8 μm silicate optical depths $\tau(9.8 \mu\text{m})$ as given in Paper II, and measures of the depression below a 12.6 $\mu\text{m}/22.9 \mu\text{m}$ baseline of the 18.1 μm (filled circles) and 19.8 μm (open circles) points. The uncertainties are ± 0.4 in $\tau(9.8 \mu\text{m})$ and ± 0.06 in $\Delta \log F_{\lambda}$ (18.1 μm , 19.8 μm).

Wynn-Williams and Becklin 1974). Several authors have recently shown that, when allowance is made for this absorption, the true 1-25 μm luminosity may be as much as 3-4 times greater than that observed before correction (e.g., Gillett *et al.* 1975; Paper II). In this section, we combine the results of Papers I and II with the new sources presented here to discuss the energetics of these uniformly observed sources. Also, with the 40-350 μm data of Emerson, Jennings, and Moorwood (1973) and Furniss, Jennings, and Moorwood (1975), we are in a position to compare the apparent ionizing photon luminosities, the bolometric luminosities, and that fraction of the energy output which is absorbed and reradiated in the 1-25 μm region.

For the new sources, the integrated fluxes *uncorrected* for silicate absorption (Table 1), together with mean observed 10-20 μm colors, were used in deriving the apparent 1-25 μm luminosities in a manner similar to that described in Paper I. Approximate corrections for the emission absorbed by silicate particles in the 10 μm and 20 μm windows were then found, using the values of $\tau(9.8 \mu\text{m})$ from Paper II. It is implicitly assumed that the silicate particles absorbing the energy in these windows reradiate it at wavelengths longer than 25 μm . The correction to the observed 20 μm flux for absorption by silicate particles is assumed to be one-third the 10 μm correction. The *corrected* luminosities are given in Table 6 and are reduced to solar units via the distances given in Table 1 and Paper I. Aside from errors in the distances, the final numbers are probably uncertain by an additional factor of 2, both because of the approximate correction for silicate absorption and because the technique of observation discriminates against low-surface-brightness extended emission. The average factor by which the integrated 1-25 μm fluxes increase is 3.

L_{α} photons are expected to be the most efficient heating mechanism for the dust particles within the H II region. Thus we compare the 1-25 μm luminosities of the H II regions with the L_{α} luminosity. We assume each ionizing photon produces one L_{α} photon, which is subsequently absorbed by dust

TABLE 6
H II REGION FLUXES AND LUMINOSITIES[†]

Galactic Source Designation	Log [Flux Wm ⁻²]			Log (L/L _⊙)				Number of Stars	
	1-25μ	Lyman α	40-350μ	1-25μ	Lyman α	40-350μ	Stars		
G268.0-1.0	-8.82	-8.58	-8.38	5.0	5.3	5.5	5.9	1	05
G274.0-1.1	-9.85	-9.35	...	5.3	5.8	...	6.4	3	05
G282.0-1.2	-9.82	-9.32	...	5.3	5.9	...	6.5	3.7	05
G285.3-0.0	-10.01	-9.56	...	4.9	5.3	...	5.9	1	05
G291.3-0.7	-8.68	-8.75	...	5.9	5.9	...	6.5	3.7	05
G291.6-0.5	-8.55	-8.52	...	6.8	6.8	...	7.3	17	04
G298.2-0.3	-9.25	-9.27	...	6.4	6.4	...	6.9	6.8	04
G327.3-0.6	-9.18	-9.04	-8.70	5.4	5.5	5.9	6.1	1.5	05
G333.1-0.4	-9.47	-9.34	-8.64	5.1	5.3	6.0	5.9	1	05
G333.3-0.4	-9.27	-9.15	-8.73	5.4	5.5	5.9	6.1	1.5	05
G333.6-0.2	-8.70	-8.80	-8.31	6.1	6.0	6.5	6.5	2.7	04
G336.5-1.5	-9.29	-9.85	...	4.8	4.3	...	5.1	1	07.5
G337.9-0.5	-9.03	-9.44	-8.77	5.5	5.1	5.8	5.7	1	05.5
G340.8-1.0	-9.85	-9.69	...	4.4	4.6	...	5.4	1	06.5
G345.4-0.9	-9.14	-9.22	-8.68	5.7	5.7	6.2	6.3	2.3	05
G348.2-1.0	-9.49	-9.75	...	5.4	5.1	...	5.7	1	05.5
G348.7-1.0	-8.92	-9.15	-8.62	6.0	5.7	6.3	6.3	2.3	05
G351.6-1.3	-9.57	{ -9.81 -9.12 }	-8.61	5.3	{ 5.1 5.8 }	6.3	{ 5.7 6.4 }	1 3	{ 05.5 05 } ¹
G353.2+0.9	-8.62	{ -9.17 -8.76 }	-8.52	4.9	{ 4.3 4.8 }	5.0	{ 5.1 5.6 }	1	{ 07.5 06 } ²
G10.2-0.3	> -10.0	-8.96	...	> 5.4	6.4	...	6.9	6.8	04
G12.8-0.2	-9.96	{ -10.01 -9.28 }	...	4.9	{ 4.8 5.5 }	...	{ 5.6 5.1 }	1 1.5	{ 06 05 } ³

[†]F(1-25μ) is the value corrected for silicate absorption. F(Ly α) is from the formula of Rubin (1968), the data in Tables 1 of Paper I and here, or the 8900 MHz data of McGee *et al.* (1975). F(40-350μ) is from Emerson *et al.* (1973) or Furniss *et al.* (1975). The luminosities use the distances given in Tables 1 of Paper I and here. The equivalent number and luminosities of the exciting stars are from L (Lyman α) and the tabulations of Panagia (1973). No corrections have been applied for 2-photon emission.

¹The smaller of the two values in brackets refers to a higher frequency measurement of a compact component by Brown and Broderick (1973). This value was used for the comparison with L (1-25μ) and the larger value was used for the comparison with L (40-350μ), in figures 14 and 15 respectively.

²Same as (1) except the higher frequency measurement is from Schraml and Mezger (1969).

³Same as (1) with high frequency measurement from Balick (1972).

particles before being converted to the two-photon continuum. With the resulting values for the L_α luminosities (Table 6), it is possible to enter the tables of Panagia (1973) and extract the number of early-type stars required to supply the ionizing flux for the H II regions, assuming a geometrical dilution factor of unity. We further assumed that the exciting stars are most likely to be class V stars. The choice of spectral type was arbitrary but does not affect the semi-quantitative nature of the discussion, since the ratio

of bolometric to ionizing photon luminosity is not a strong function of luminosity for the earlier O stars. Figure 14 compares the 1-25 μm and the L_α luminosities from Table 6. The only difference between this figure and a similar figure in Paper I is that the correction for silicate absorption has moved the points closer to the line of equality. Figure 14 shows that *to within a factor of 2, the 1-25 μm luminosity of the H II regions considered here and in Paper I can be accounted for by absorption by dust of L_α photons.* Although a plot of

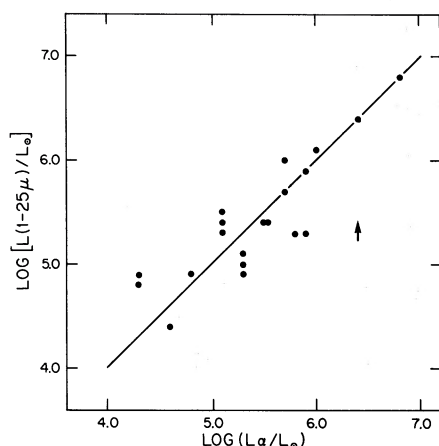


FIG. 14.—Relation between the 1–25 μm luminosity as approximately corrected for silicate absorption at 10 μm and 20 μm , and the luminosity in $L\alpha$ photons as calculated from observed radio flux densities for 21 H II regions. See text for discussion of these computations. The uncertainties are of order ± 0.5 in $\log [L(1-25 \mu\text{m})/L_{\odot}]$. The straight line is one of equal luminosity. The single arrow represents W31, for which only a lower limit to the 1–25 μm flux density was available.

$L(1-25 \mu\text{m})$ versus $L(40-350 \mu\text{m})$ (Emerson, Jennings, and Moorwood 1973; Furniss, Jennings, and Moorwood 1975) has a considerable amount of scatter, the two quantities are roughly proportional to each other.

To investigate the bolometric luminosities, we have extracted, from the lists of Emerson, Jennings, and Moorwood (1973) and Furniss, Jennings, and Moorwood (1975), all of the sources with *calculated* 40–350 μm luminosities and with 5 GHz flux densities given by Shaver and Goss (1970). We have restricted ourselves to just these references, since the uniformity of the measurements will minimize scatter due to varying instrumental sensitivity, beamwidth, etc. The formula of Rubin (1968) and the tables of Panagia (1973) were again used to obtain the number and total bolometric luminosities of the early-type stars required to provide the observed 5 GHz luminosity. Figure 15 is a plot similar to that given by Wynn-Williams and Becklin (1974). The conclusion of Wynn-Williams and Becklin and of Paper I is further supported: *within the uncertainties, there is no evidence that any significant fraction of the primary stellar ionizing flux is being absorbed directly by the dust* either within or around the H II regions.³ Examples to the contrary given by Furniss, Jennings, and Moorwood (1975) can be encompassed within the uncertainties. It is interesting that the linear relations in Figures 14 and 15 hold over two orders of magnitude.

The above discussion has been based on several important and probably unrealistic simplifying assumptions about the relative distributions of stars, dust, and gas. The observational evidence points to a more or less continuous range of dust temperature and

³ If any of the 40–350 μm radiation is derived from non-ionizing stars, then this conclusion is strengthened.

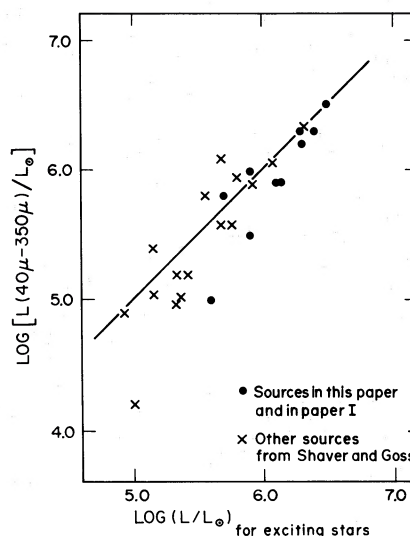


FIG. 15.—Relation between the measured far-infrared luminosities and the total stellar luminosities of H II regions as calculated from radio data and models for early-type stars. See text for discussion. The straight line is one of equal luminosity.

distribution within and around the ionized region (e.g., the similarity between radio and 40–350 μm maps presented by Emerson, Jennings, and Moorwood 1973). If the far-infrared emission were confined to circumnebular molecular clouds, maps at these wavelengths would reveal shell structure. Thus the division of dust into two spatial components and the arbitrary cutoff at 25 μm are artificial. In particular, we note that the recent results of Harper *et al.* (1976) indicate that most of the radiation at 100 μm from M17 is coming from the same region as the 10 μm and 20 μm emission.

VII. SUMMARY AND CONCLUSIONS

In this paper we have presented 1.2–20 μm observations of nine southern H II regions which had not been observed previously. The main results which we have found are:

1. NGC 3603 is a striking example of an H II region in which the 10 μm and 20 μm emission corresponds spatially with the $H\alpha$ emission. An immediate implication of this observation is that there are no significant absorbing clouds along the line of sight to the most intense parts of this source.

The relative spatial distribution of the compact cluster of luminous O stars, the ionized gas, and the dust which emits at 10 μm and 20 μm are evidence for a dynamical interaction between these components in the sense that the stars have cleared out a volume of space in their immediate vicinity.

2. Several stellar sources have been found near some of the IR/H II complexes. Although their physical association with the corresponding H II regions is not established, a few of them may be late-type supergiants, while one of them, NGC 3603/IRS-9, is either

a star with a very thick circumstellar shell or a relatively hot (~ 1000 K) blackbody.

3. We have reexamined the energetics of IR/H II regions, using our 1–25 μm data and published 40–350 μm data. Again, we find support for the conclusions of Paper I; viz., to within the uncertainties, a significant fraction of the 1–25 μm emission (that from the hotter particles) can be accounted for by resonantly trapped $L\alpha$ photons (the most efficient energy input mechanism). Second, the total luminosities of the H II regions are, to within a factor of 2, consistent with those predicted from ionizing photon luminosities, which in turn are calculated from radio observations.

Thus the dust which emits in the 1–350 μm region, regardless of its location, does not affect the total ionization rate by more than a factor of 2 (cf. Wynn-Williams and Becklin 1974).

We thank Dr. H. W. Babcock for his support of our Guest Observer programs at Las Campanas. We thank Dr. N. R. Walborn for a copy of his 4 m plate of NGC 3603. Comments by Dr. G. Neugebauer have clarified the presentation. We appreciate the assistance of Srs. Papic and Guerra. Also, we appreciate the travel funds made available over several years by Harvard College Observatory.

REFERENCES

- Baldwin, J. R., Frogel, J. A., and Persson, S. E. 1973, *Ap. J.*, **184**, 427.
 Balick, B. 1972, *Ap. J.*, **176**, 353.
 Beard, M., Thomas, B. MacA., and Day, G. A. 1969, *Australian J. Phys.*, *Ap. Suppl.*, No. 11, p. 27.
 Becklin, E. E., Beckwith, S., Gatley, I., Matthews, K., Neugebauer, G., Sarazin, C., and Werner, M. W. 1976, *Ap. J.*, **207**, 770.
 Becklin, E. E., Frogel, J. A., Kleinmann, D. E., Neugebauer, G., Persson, S. E., and Wynn-Williams, C. G. 1974, *Ap. J.*, **187**, 487.
 Becklin, E. E., Frogel, J. A., Neugebauer, G., Persson, S. E., and Wynn-Williams, C. G. 1973a, *Ap. J. (Letters)*, **182**, L125.
 Becklin, E. E., Hansen, O., Kieffer, H., and Neugebauer, G. 1973b, *A.J.*, **78**, 1063.
 Blaauw, A. 1963, in *Basic Astronomical Data*, ed. K. Aa. Strand (Chicago: University of Chicago Press), p. 383.
 Caswell, J. L. 1972, *Australian J. Phys.*, **25**, 443.
 Caswell, J. L., Batchelor, R. A., Haynes, R. F., and Huchtmeier, W. K. 1974, *Australian J. Phys.*, **27**, 417.
 Caswell, J. L., and Haynes, R. F. 1975, *M.N.R.A.S.*, **173**, 649.
 Caswell, J. L., Murray, J. D., Roger, R. S., Cole, D. J., and Cooke, D. J. 1976, *Astr. Ap.*, **45**, 239.
 Caswell, J. L., and Robinson, B. J. 1974, *Australian J. Phys.*, **27**, 597.
 Churchwell, E. 1974, in *IAU Symposium No. 60, Galactic Radio Astronomy*, ed. F. J. Kerr and S. C. Simonson, III (Dordrecht: Reidel), p. 195.
 Cohen, J. G., and Frogel, J. A. 1976, private communication.
 Elmegreen, B., and Lada, C. J. 1976, preprint.
 Emerson, J. P., Jennings, R. E., and Moorwood, A. F. M. 1973, *Ap. J.*, **184**, 401.
 Frogel, J. A., and Persson, S. E. 1974, *Ap. J.*, **192**, 351 (Paper I).
 ———. 1975, *Ap. J.*, **197**, 351.
 Furniss, I., Jennings, R. E., and Moorwood, A. F. M. 1975, *Ap. J.*, **202**, 400.
 Gillett, F. C., Forrest, W. F., Merrill, K. M., Capps, R. W., and Soifer, B. T. 1975, *Ap. J.*, **200**, 609.
 Goss, W. M., and Radhakrishnan, V. 1969, *Ap. Letters*, **4**, 199.
 Goss, W. M., and Shaver, P. A. 1970, *Australian J. Phys.*, *Ap. Suppl.*, No. 14, p. 1.
 Harper, D. A., Low, F. J., Rieke, G. H., and Thronson, H. A. 1976, *Ap. J.*, **205**, 136.
 Houck, J. 1976, private communication.
 Hyland, A. R., Becklin, E. E., Frogel, J. A., and Neugebauer, G. 1972, *Astr. Ap.*, **16**, 204.
 Johnson, H. L. 1966, *Ann. Rev. Astr. Ap.*, **4**, 193.
 ———. 1968, in *Nebulae and Interstellar Matter*, ed. B. M. Middlehurst and L. H. Aller (Chicago: University of Chicago Press), p. 167.
 Johnston, K. J., Robinson, B. J., Caswell, J. L., and Batchelor, R. A. 1972, *Ap. Letters*, **10**, 93.
 Lee, T. A. 1970, *Ap. J.*, **217**, 162.
 McGee, R. X., Newton, L. M., and Batchelor, R. A. 1975, *Australian J. Phys.*, **28**, 185.
 Moffat, A. F. J. 1974, *Astr. Ap.*, **35**, 315.
 Panagia, N. 1973, *A.J.*, **78**, 929.
 Perek, L., and Kohoutek, L. 1967, *Catalogue of Galactic Planetary Nebulae* (Prague: Academy of Sciences) (CGPN).
 Persson, S. E., Frogel, J. A., and Aaronson, M. 1976, *Ap. J.*, **208**, 753 (Paper II).
 Radhakrishnan, V., Goss, W. M., Murray, J. D., and Brooks, J. W. 1972, *Ap. J. Suppl.*, **24**, 49.
 Robinson, B. J., Caswell, J. L., and Goss, W. M. 1974, *Australian J. Phys.*, **27**, 575.
 Rubin, R. H. 1968, *Ap. J.*, **154**, 391.
 ———. 1970, *Astr. Ap.*, **8**, 171.
 Schraml, J., and Mezger, P. G. 1969, *Ap. J.*, **156**, 269.
 Shaver, P. A., and Goss, W. M. 1970, *Australian J. Phys.*, *Ap. Suppl.*, No. 14, p. 133.
 Sher, D. 1965, *M.N.R.A.S.*, **129**, 237.
 Walborn, N. R. 1973, *Ap. J. (Letters)*, **182**, L21.
 Wynn-Williams, C. G., and Becklin, E. E. 1974, *Pub. A.S.P.*, **86**, 5.
 Wynn-Williams, C. G., Becklin, E. E., and Neugebauer, G. 1972, *M.N.R.A.S.*, **160**, 1.

MARC AARONSON: Harvard College Observatory, 60 Garden Street, Cambridge, MA 02138

JAY A. FROGEL: Cerro Tololo Inter-American Observatory, P.O. Box 26732, Tucson, AZ 85726

S. ERIC PERSSON: Hale Observatories, 813 Santa Barbara Street, Pasadena, CA 91101

PLATE 14



Fig. 2.—H α plus forbidden N photograph of the NGC 3603 region taken by N. Walborn on the CTIO 4 m telescope. The superposed contour map is the 10 μ m map of Fig. 3.

FROGEL *et al.* (see page 725)